

# Influence of ground roughness on the wake of a yawed wind turbine - a comparison of wind-tunnel measurements and model predictions

**Victor P. Stein, Hans-Jakob Kaltenbach**

Fachgebiet Strömungsbeeinflussung und Aeroakustik, Fakultät Maschinenwesen  
Technische Universität München, Boltzmannstr. 15, 85748 Garching

E-mail: [victor.stein@aer.mw.tum.de](mailto:victor.stein@aer.mw.tum.de), [hans-jakob.kaltenbach@tum.de](mailto:hans-jakob.kaltenbach@tum.de)

**Abstract.** Wind-tunnel measurements in the wake of a three bladed horizontal axis wind turbine model (HAWT) operating in yawed conditions are presented. Measurements are made at a constant tip speed ratio within two neutrally-stratified turbulent boundary layers of different aerodynamic roughness length to investigate its influence on the wake trajectory. It is found that the wake is less deflected with increasing terrain roughness. The recorded flow field is then used to assess the predictive capability of two analytical wake models.

## 1. Introduction

Control of the wake trajectory by means of yaw misalignment has recently raised attention as a possibility to increase the energy production of wind farms. In this control strategy the wake of a wind turbine is deflected to the side by an intentional yaw misalignment to alleviate the losses of downstream turbines which would otherwise operate in the wake of the upwind turbine. Fleming et al. [1] used large-eddy simulation (LES) to study different wake control strategies, showing that yawing a turbine is an effective method to redirect the wake. Vollmer & Steinfeld [2] also used LES to study the wake deflection in atmospheric boundary layers with different thermal stability. They showed that, for a given yaw angle and decreasing atmospheric stability, the wake deflects less whereas the variance of its trajectory increases. Based on the results of wind tunnel measurements of a yawed model wind turbine within a turbulent boundary layer, Bastankhah & Porté-Agel [3] derived an analytical model for the prediction of the wake deflection. The model predicts the wake deflection, amongst other parameters, as a function of the turbulence intensity, showing a decrease in the wake deflection with increasing turbulence intensity.

The aim of the present work is twofold: the first is to identify the role of the change of turbulence intensity on the wake development behind a yawed model wind turbine immersed in two turbulent boundary layers of different aerodynamic roughness length; the second is to analyse the predictive capability of two selected analytical wake models regarding the wake recovery and deflection within these two boundary layers.

## 2. Experimental Set-up

### 2.1. Wind Tunnel and Instrumentation

The experiments are performed at the chair of aerodynamics closed-loop boundary layer wind tunnel. The test section is 2.7 m wide, 1.8 m high and 21 m long. To ensure a zero axial



pressure gradient the wind tunnel ceiling is inclined. An atmospheric boundary layer is simulated using Counihan's technique [4], where different arrangements of vertical fins, vortex generators and distributed roughness on the wind tunnel floor result in a family of mean flow profiles  $U(z) \sim (z/z_0)^\alpha$  characterized by certain values of shear exponent  $\alpha$  and roughness length  $z_0$ . Throughout this paper,  $z$  denotes the wall-normal,  $x$  the axial and  $y$  the lateral coordinate. Instantaneous velocities are measured using a triple hot-wire probe which is made of  $5\mu\text{m}$  gold-coated tungsten wires of 3mm length. The probe is connected to a ten-channel AALAB AN 1003 anemometer system. Each channel consists of a Wheatstone bridge, an amplifier and a low-pass filter with a 1kHz cut-off frequency. Velocity signals are sampled at 3 kHz using a 12-bit digitizer Data Translation DT2821 with a record length of 120 s. With this configuration a relative error of the velocity measurement of  $\epsilon_u < 3\%$  is obtained, see [5]. The mean velocity at hub height  $U_{hub}$  is measured simultaneously by means of a Prandtl tube, located at a position upstream of the wind turbine at which no flow displacement due to the turbine itself is noticeable.

## 2.2. Boundary Layer Characteristics

In the current study, the wind turbine model is located approximately 12.5 meters downstream of the fins where the boundary layer thickness is  $\delta \approx 1.5$  m. To generate boundary layers of different aerodynamic roughness length  $z_0$  and mean wind shear exponent  $\alpha$ , the distribution density of the roughness elements, consisting of staggered Lego brick columns, is varied. For the presented boundary layers, named smooth (SBL) and rough boundary layer (RBL) in the following, the parameters  $\alpha = 0.16/0.32$  and  $z_0 = 0.53/3.3$  mm were determined by fitting a logarithmic and a power law velocity profile to the measured average velocity  $\bar{u}$ . The turbulence intensity at hub height  $z_h = 450$  mm is  $I_u(z_h) = 0.09$  and  $I_u(z_h) = 0.15$ , respectively. At a scale of  $1:\mathcal{O}(350)$  these parameters represent neutrally-stratified turbulent boundary layers over grass land and forested terrain with  $z_0 = 0.19/1.16$  m. Figure 1 shows the vertical profiles of the (a) mean velocity, (b) its variance  $\overline{u'^2}$  and (c) shear stress  $-\overline{u'w'}$  measured in the boundary layer using the hub height  $z_h$  and the mean velocity of the undisturbed boundary layer  $\bar{u}_\infty(z_h)$  at this location as reference. Additionally, the longitudinal length scales are compared with Counihan's empirical expression  $L_u^x = Cz^\alpha$  [6] in figure (d). The results show, that the length scales in the wind tunnel follow the

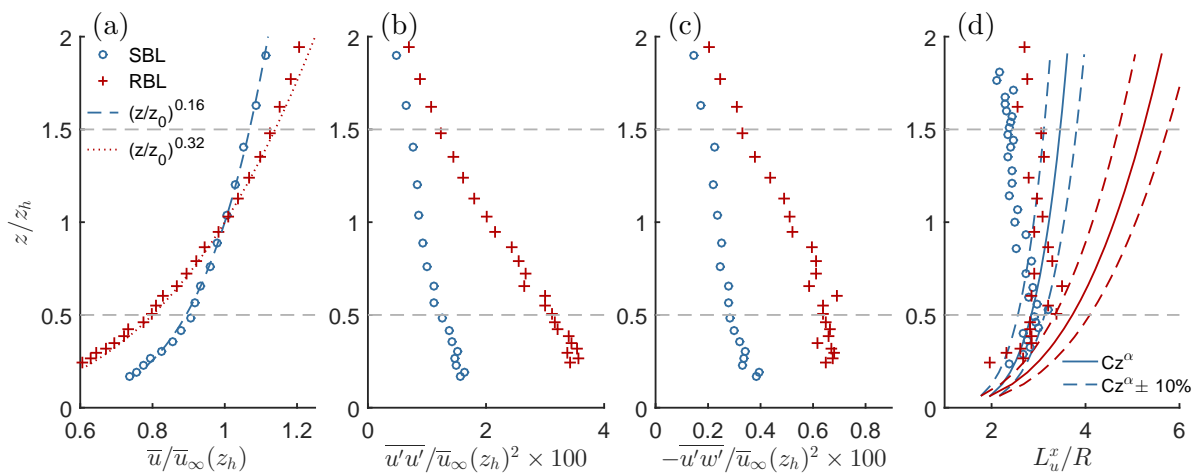


**Figure 1.** (a) mean velocity in axial direction  $\bar{u}$ , (b) axial turbulence intensity  $\overline{u'w'}$  and (c) shear stress  $-\overline{u'w'}$  within the SBL (blue line) and RBL (red line), all normalised by the mean velocity at hub height of the undisturbed boundary layer  $\bar{u}_\infty(z_h)$ . (d) longitudinal integral length scale  $L_u^x$  normalised by the rotor radius  $R$ . The horizontal dashed lines indicate the rotor edges.

correct trend up to half of the hub height  $z_h$ . Above this region length scales decrease slightly in size reaching a constant value. At the upper edge of the rotor disc the relative deviation of the length scale is about 30%. Throughout all presented measurements the roughness Reynolds number,  $Re_\tau = u_\tau z_0/\nu$ , where  $\nu$  is the kinematic viscosity, is  $Re_\tau = 19$  and  $190$  in the smooth and rough boundary layer respectively, which falls well above the lower limit of 1 suggested by Heist & Castro [7]. Chamorro et al. [8] suggest a Reynolds number independence of the wake of a model wind turbine on the basis of the rotor diameter  $D$  at  $Re_D = \bar{u}_\infty(z_h)D/\nu > 9.3 \times 10^4$  which is about an order less than within the presented measurements where  $Re_D = 3.04 \times 10^5$ . Hence the surface can be considered as aerodynamically rough and main flow statistics should be independent of the Reynolds number.

### 2.3. Model Wind Turbine

The wind turbine model is a three-bladed HAWT with a rotor diameter of  $D$  and equal hub height  $z_h = D = 2R = 450$  mm, corresponding to a full scale rotor radius of 80 m. Blocking effects are considered to be negligible since the blockage ratio of the rotor is 4.2% (i.e., the ratio of the blade swept area to the tunnel cross section area excluding the area covered by the boundary layers at the sidewalls and ceiling). Due to the naturally evolving boundary layers at the sidewalls, the lateral and the vertical spreading of the wake can be influenced after a certain distance behind the rotor. At the furthest downstream position from which profiles are presented the distance between the edges of the wake and side wall boundary layers exceeds  $1.5R$ . Furthermore, no asymmetry is observed in the profiles of mean flow and Reynolds stresses, despite the fact that the wake center has shifted by 7% of the tunnel width away from the tunnel axis. If a significant influence of the side walls were present we would have expected asymmetric profiles. Sideward wake deflections of similar magnitude have also been observed in the LES of Vollmer & Steinfeld [2] for a full scale wind turbine immersed within a neutrally-stratified boundary layer with a roughness comparable to the presented smooth boundary layer. This simulation is virtually free of “sidewall effects”, implying that the spatial wake development measured in the wind-tunnel is indeed a good approximation of the real situation.

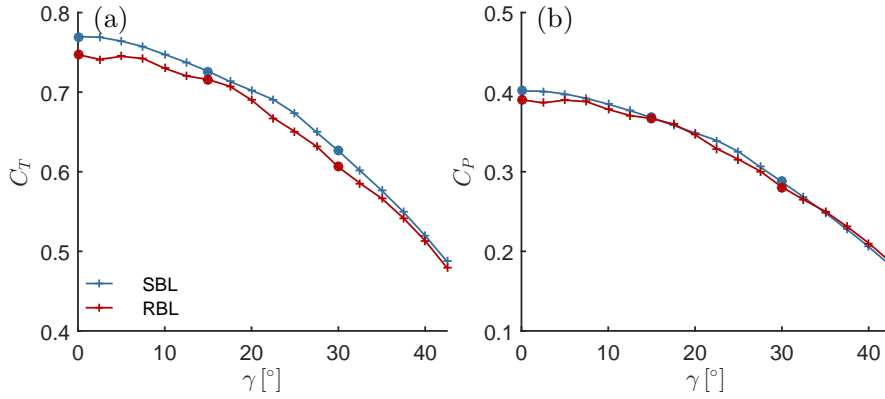
The generated thrust is measured by means of a strain gauge installed between nacelle and tower. Thus, the measurement includes axial component of forces on the blades, spinner and nacelle. The torque produced at the rotor blades is estimated from the electric current of the generator. To improve the accuracy of this approach the measurement setup is calibrated by using the torque meter rig developed by Bastankhah & Porté-Agel [9]. Within the presented measurements the wind turbine is operating at the design tip speed ratio of  $\lambda_{dsg} = 6.5$  for which the angular frequency  $\Omega$  of the rotor is kept constant with a standard deviation of  $< 0.25\%$ . More details on the design of the wind turbine model are given in [10]. Thrust and power coefficient are defined as

$$C_T = \frac{T}{\frac{1}{2}\rho A \bar{u}_\infty^2(z_h)} \quad \text{and} \quad C_P = \frac{\Omega Q}{\frac{1}{2}\rho A \bar{u}_\infty^3(z_h)}, \quad (1)$$

where  $T$  and  $Q$  are the produced thrust and torque at the rotor,  $\rho$  the density of the air and  $A$  the blade swept area. Resulting coefficients against yaw angle  $\gamma$  measured at the design tip speed ratio  $\lambda_{dsg}$  are shown in figure 2.

### 3. Analytical Wake Models

In this section the analytical wake models derived by Bastankhah & Porté-Agel [3], named Model B in the following, as well as the model derived by Jiménez & Crespo [11], named Model J in the following, are briefly described. These models have been chosen for comparison with the measurement results, since both are based on mass conservation, as well as conservation of streamwise and spanwise momentum.

**Figure 2.**

(a) Thrust and (b) power coefficients as function of yaw angle  $\gamma$  measured at  $\lambda_{dsg}$  for the SBL (blue lines) and RBL (red lines). For coloured points hot wire measurements in the wake were performed.

### 3.1. Wake model of Bastankhah & Porté-Agel (Model B)

The model separates the wake in a potential core and a far wake region. It assumes a two-dimensional Gaussian profile for the velocity deficit in the far wake

$$\Delta u_B = \frac{\bar{u}_\infty - \bar{u}}{\bar{u}_\infty} = \begin{cases} \Delta u_{C,B} & x < x_0, r \leq r_{pc} \\ \Delta u_{C,B} e^{-0.5((r-r_{pc})/s)^2} & x < x_0, r > r_{pc} \\ \Delta u_{C,B} e^{-0.5((y-y_C)/\sigma_y)^2} e^{-0.5((z-z_h)/\sigma_z)^2} & x > x_0 \end{cases} \quad (2)$$

where  $\Delta u_C$  is the centreline velocity deficit,  $r_{pc}$  is the potential core radius at each  $x$ ,  $r$  is the lateral distance from the wake centre,  $s$  denotes the characteristic width of the shear layer (which increases from  $s = 0$  at  $x = 0$  to  $s = \sigma_{y0}$  at  $x = x_0$ ),  $y_C$  is the centreline position in the horizontal plane, and  $\sigma_y$  and  $\sigma_z$  are the lateral and vertical wake half width. The onset of the far wake  $x_0$  is estimated as

$$\frac{x_0}{R} = \frac{\sqrt{2} \cos(\gamma) (1 + \sqrt{1 - C_T})}{(\alpha^* I_u(z_h) + \beta^* (1 - \sqrt{1 - C_T}))} \quad (3)$$

**Table 1.** Far wake onset  $x_0/R$ 

BL / $\gamma$	0°	15°	30°
SBL	7.28	7.33	7.33
RBL	4.96	4.97	4.98

where  $\alpha^* = 2.32$  and  $\beta^* = 0.154$ . The resulting locations  $x_0$  for both boundary layers and various yaw angles are given in table 1. It can be noticed, that the dependency of the predicted far wake onset regarding the yaw angle is rather negligible, whereas, due to the different degree of turbulence intensity  $I_u$ ,  $x_0$  is significantly different for both boundary layers.

In the far wake the model assumes a linear growth of the lateral and vertical wake half widths

$$\sigma_y = k_y(x - x_0) + \sigma_{y0} \quad \text{and} \quad \sigma_z = k_z(x - x_0) + \sigma_{z0}, \quad (4)$$

where  $k_y$  and  $k_z$  are the spreading rates in lateral and vertical direction, and  $\sigma_{y0} = R \cos(\gamma)/\sqrt{2}$  and  $\sigma_{z0} = R/\sqrt{2}$ . In order to simplify the calculation of the wake center velocity deficit  $\Delta u_{C,B}$  and skew angle  $\Theta_{C,B} = \bar{v}(y_C)/\bar{u}(y_C)$ , the wake half widths  $\sigma_y$  and  $\sigma_z$  are combined in an isotropic wake width

$$\bar{\sigma}_B = \bar{k}_B(x - x_0) + \bar{\sigma}_0, \quad \bar{k}_B = \sqrt{k_y k_z} \quad \text{and} \quad \bar{\sigma}_0 = \sqrt{\sigma_{y0} \sigma_{z0}}. \quad (5)$$

The wake centre velocity deficit  $\Delta u_{C,B}$  and skew angle  $\Theta_{C,B}$  in the far wake region are then derived by assuming conservation of momentum in streamwise and spanwise direction, which

results in

$$\Delta u_{C,B} = \begin{cases} \Delta u_{C,0} & x < x_0 \\ 1 - \sqrt{1 - \frac{C_T \cos(\gamma)}{2(\bar{\sigma}_B/R)^2}} & x > x_0 \end{cases}, \quad \Theta_{C,B} = \begin{cases} \Theta_{C,0} & x < x_0 \\ \frac{\Theta_{C,0} \bar{\sigma}_0 E_0}{\bar{\sigma}_B^2 (\Delta u_{C,B}^2 - 3e^{1/12} \Delta u_{C,B} + 3e^{1/3})} & x > x_0 \end{cases} \quad (6)$$

with  $E_0 = \Delta u_{C,0}^2 - 3e^{1/12} \Delta u_{C,0} + 3e^{1/3}$ . In the potential core region the centreline velocity deficit  $u_{C,0} = 1 - \sqrt{1 - C_T}$  and skew angle  $\Theta_{C,0} = \frac{0.3\gamma}{\cos(\gamma)} (1 - \sqrt{1 - C_T})$  are assumed to be constant. Finally, the wake centreline in the horizontal plane can then be found by equating  $\Theta_{C,B}$  with  $dy/dx$  and integrating it as

$$y_{C,B} = \int_0^x \Theta_{C,B} dx. \quad (7)$$

It should be mentioned that this approach implies the existence of a streamline which equals the wake centreline.

### 3.2. Wake model of Jiménez & Crespo (Model J)

One of the main assumptions of the model is a uniform velocity deficit  $\Delta u$  and skew angle  $\Theta$  across the wake

$$\Delta u_J = \frac{\bar{u}_\infty - \bar{u}}{\bar{u}_\infty} = \begin{cases} \Delta u_0 & r \leq \delta/2 \\ 0 & r > \delta/2 \end{cases}, \quad \Theta = \frac{\bar{v}}{\bar{u}} = \begin{cases} \Theta_{C,J} & r \leq \delta/2 \\ 0 & r > \delta/2 \end{cases} \quad (8)$$

where  $r$  is the lateral distance from the wake centre and  $\delta$  the wake width

$$\delta = D + \beta x \quad (9)$$

which is also assumed to grow linear with the spreading rate  $\beta$ . Similar to Model B, conservation of momentum in streamwise and spanwise direction is assumed, though a first order approximation is used which gives

$$\Delta u_0 = \frac{C_T}{2} \left( \frac{D}{\delta} \right)^2 \cos(\gamma), \quad \Theta_{C,J} = \frac{C_T}{2} \left( \frac{D}{\delta} \right)^2 \sin(\gamma) \quad (10)$$

The apparent difference of eq. (10) from the formula in the original work is due to different definitions used for the thrust coefficient. As before, the wake centreline in the horizontal plane is then found by integrating the skew angle in downstream direction as in eq. (7).

Due to the different definition of the velocity deficit profile and its width, the resulting values of  $\Delta u_0$  and  $\delta$  are not directly comparable to those in Model B. However, since both models consider mass and momentum conservation it is possible to relate those quantities and to define the auxiliary variables  $\bar{\sigma}_J$  and  $\Delta u_{C,J}$ , which are then used for the comparison with the measurement results. Mass and momentum conservation in non-dimensional form result in

$$\int_{-\infty}^{\infty} \int_{-\infty}^{\infty} \Delta u dy dz = const., \quad \int_{-\infty}^{\infty} \int_{-\infty}^{\infty} \Delta u (1 - \Delta u) dy dz = const. \quad (11)$$

Inserting the predicted velocity deficits of both models eq. (2) and (8) then gives

$$\bar{\sigma}_J = \delta/4 = \bar{\sigma}_B, \quad \Delta u_{C,J} = 2\Delta u_0 = \Delta u_{C,B} \quad (12)$$

Additionally, with the assumption, that in the far wake  $\bar{k}_B x \gg \bar{\sigma}_0$  and  $\beta x \gg D$  the auxiliary spreading rate  $\bar{k}_J = \beta/4 \approx \bar{k}_B$  can be defined.

#### 4. Results

Hot wire measurements have been performed for both boundary layers with the model wind turbine operating at the design tip speed ratio  $\lambda_{dsg}$  at the yaw angles  $\gamma = 0^\circ, 15^\circ, 30^\circ$ . Thereby the velocity field has been recorded at downstream distances  $x/R = 2, 4, 6, 10, 14, 18$  within the lateral range  $-2.8 < y/R < 2.8$ . The velocity profiles along the lateral coordinate for the yaw angles  $\gamma = 0^\circ$  and  $30^\circ$  measured within both boundary layers are shown in figure 3. Just for the sake of clarity the velocity profile at  $x/R = 4$  is left out. Since the higher background turbulence in the rough boundary layer enhances the momentum exchange between the wake and the outer flow, a faster wake recovery compared to the smooth boundary layer is clearly visible for both yaw angles. Additionally, due to the enhanced momentum transfer, in the same manner the wake also loses its potential to penetrate the lateral undisturbed flow in case of a yaw misalignment and is hence less deflected as it can be seen in figure 3(b).

In the following, the recovery of the wake and its growth as well as the wake trajectory are discussed and compared with the predictions of the two analytical wake models.

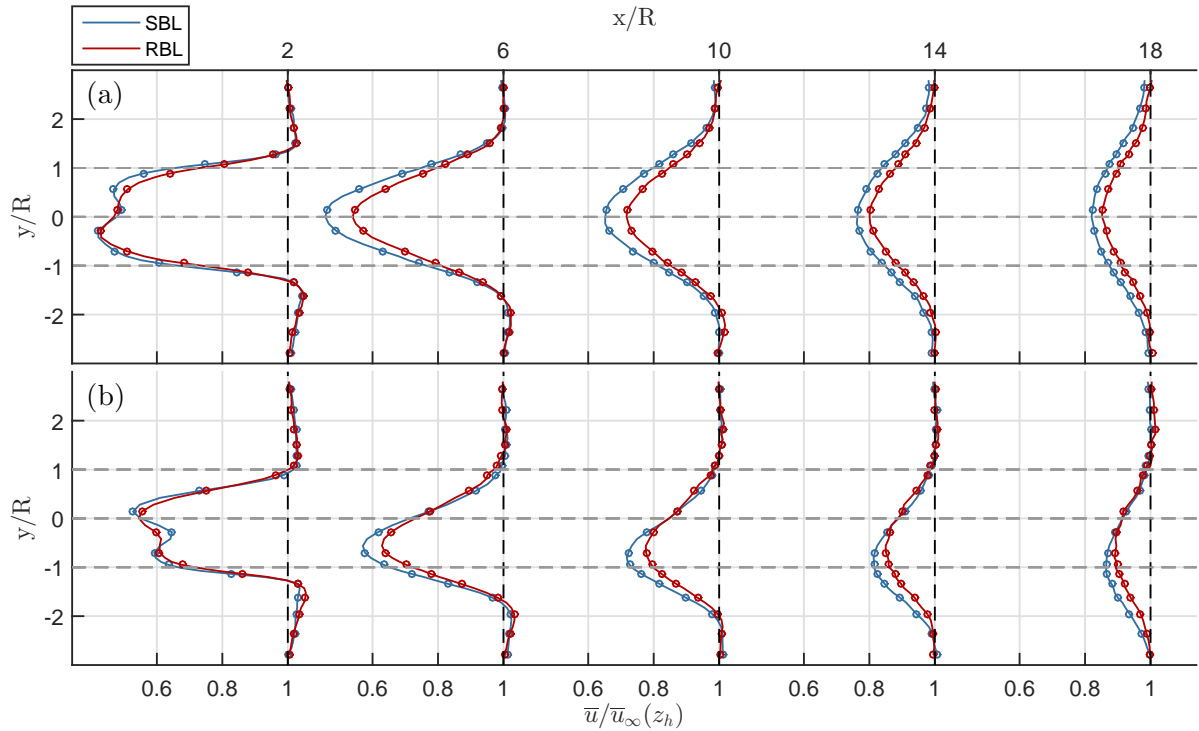


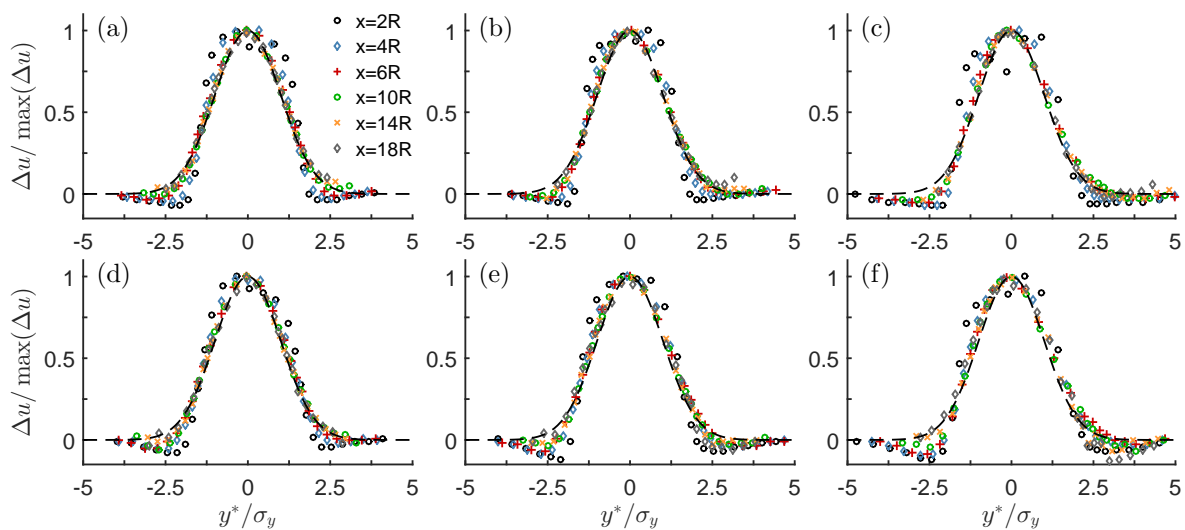
**Figure 3.** Lateral profiles of the normalised streamwise velocity  $\bar{u}/\bar{u}_\infty(z_h)$  in the wake of the model wind turbine immersed within the SBL (blue line) and RBL (red line) operating at (a)  $\gamma = 0^\circ$  and (b)  $\gamma = 30^\circ$ . The horizontal dashed lines indicate the rotor edges.

The lateral wake width  $\sigma_y$  and wake center position  $y_C$  in the horizontal plane are derived from the measurements by numerical integration of the velocity deficit and momentum deficit respectively

$$\sigma_y = \frac{1}{\sqrt{2\pi} \max(\Delta u)} \int_{-\infty}^{\infty} \Delta u \, dy \quad y_C = \frac{\int_{-\infty}^{\infty} \Delta u^2 y \, dy}{\int_{-\infty}^{\infty} \Delta u^2 \, dy}. \quad (13)$$

The vertical wake center position  $z_C$  and wake width  $\sigma_z$  are calculated analogously. To demonstrate the robustness of the used methods, profiles of the velocity deficit at different downstream positions are shown in figure 4 for all measured cases. The velocity deficit is

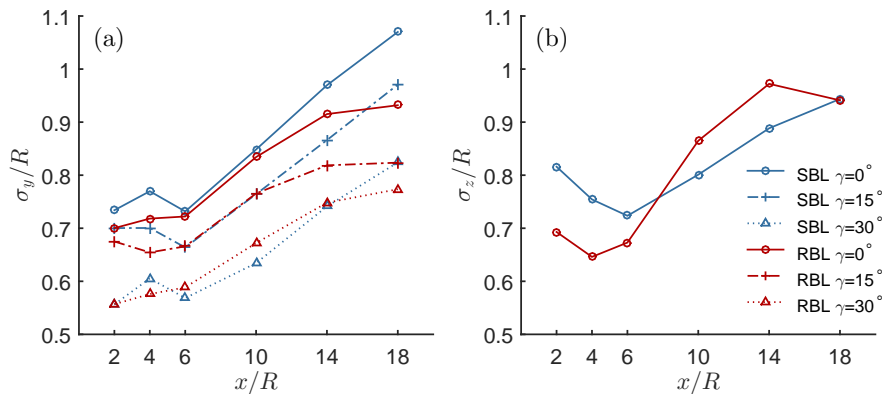
thereby normalised with the maximum deficit at the respective downstream position, whereas the lateral coordinate is represented by  $y^* = y - y_C$  and normalised by the lateral wake half width  $\sigma_y$ . As can be seen from the figure all profiles nearly collapse on to a single curve, which can be approximated by a Gaussian distribution, shown as *black dashed line*, and therewith become self-similar. In the case of the smooth boundary layer this is true for distances  $x/R \geq 6$ . Due to the faster wake recovery in case of the rough boundary layer, the velocity deficit profiles in this case become self-similar in even smaller distances. It should be noted, that the almost perfect symmetry of the profiles indicates that any interference of the wake with the wind-tunnel side walls is negligible. For the highest yaw angle the profiles become slightly skewed. This is unlikely to be caused by wall interference since it is discernible at all measurement stations and hence occurs for different distances to the side wall.



**Figure 4.** Lateral profiles of the normalised velocity deficit  $\Delta u/\max(\Delta u)$  in the wake of the model wind turbine immersed in the SBL with (a)  $\gamma = 0^\circ$ , (b)  $\gamma = 15^\circ$ , (c)  $\gamma = 30^\circ$  and in the RBL with (d)  $\gamma = 0^\circ$ , (e)  $\gamma = 15^\circ$ , (f)  $\gamma = 30^\circ$ . *Black dashed line* denotes Gaussian distribution  $e^{-0.5(y^*/\sigma_y)^2}$ . The *legend* indicates the downstream position.

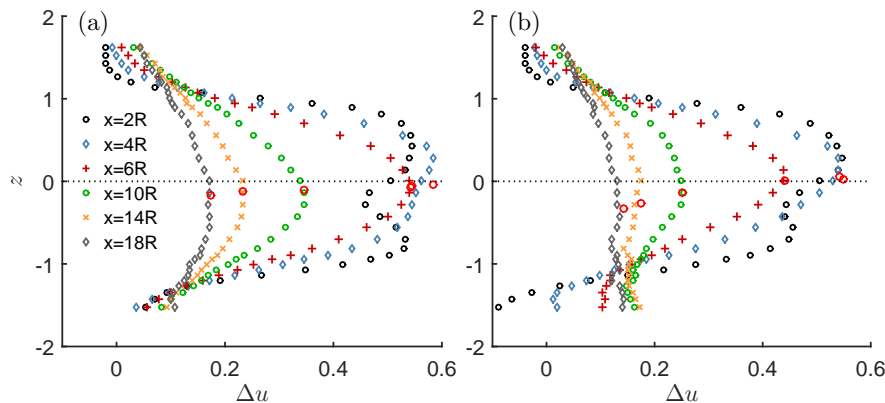
The downstream evolution of the lateral wake width  $\sigma_y$  for all measured yaw angles and flow conditions is shown in figure 5(a). Since hot wire measurements were also performed in the vertical plane for un-yawed conditions in both boundary layers, the vertical wake width  $\sigma_z$  for these cases are shown in figure 5(b). For the smooth boundary layer, both vertical and lateral wake width exhibit the well known linear wake growth, which holds for all measured yaw angles. All smooth cases show the nearly identical lateral spreading rate  $k_y = d\sigma_y/dx$ . These findings are in accordance with the results of Bastankhah & Porté-Agel [3]. For the rough boundary layer the vertical wake width grows faster than in the smooth case, which is also in agreement with the LES study of Wu & Porté-Agel [12] and the experimental investigation of Jin & Chamorro [13] et. al. However, the lateral wake width is smaller than in the smooth case. Furthermore, both lateral and vertical growth rates decrease for downstream distances  $x/R > 10$ . The latter can be argued to be caused by an interaction of the wake with the roughness elements on the wind tunnel floor.

Figure 6 shows the velocity deficit for un-yawed conditions in the vertical plane for the (a) smooth and (b) rough boundary layer. The vertical position of the momentum deficit center  $z_C$  is thereby marked by *red dots*. For the smooth boundary layer the velocity deficit in the vertical plane also exhibits an approximately Gaussian shaped distribution in the far wake.



**Figure 5.** Wake half width in (a) lateral and (b) vertical direction. The *legend* indicates flow condition and yaw angle for both subfigures.

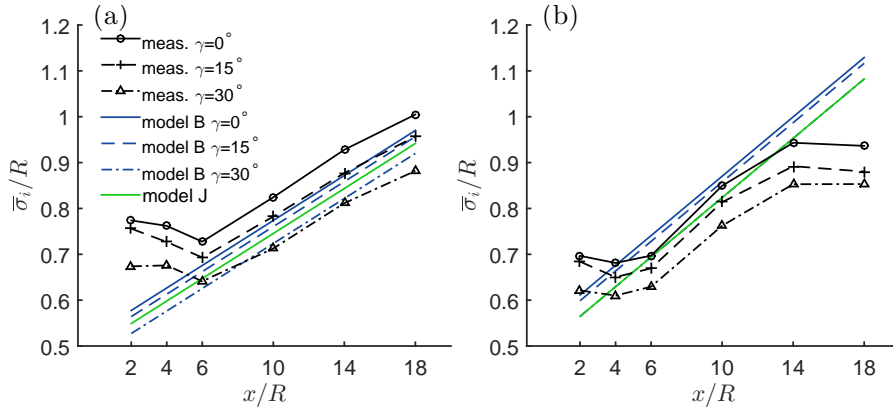
This distribution is just distorted in the region below the bottom tip at a distance of  $x/R = 18$ , whereas in the case of the rough boundary layer this distortion can already be observed for distances  $x/R \geq 10$ . The authors think that this is a result of an interaction of the wake with the ground. Due to this interaction flow momentum near the ground is lost by friction, which in turn leads to a drop of the momentum deficit center. Such a change in the momentum deficit in the wake is likely to affect the wake development and hence the wake growth.



**Figure 6.** Vertical profiles of the velocity deficit in the wake of the un-yawed model wind turbine immersed in the (a) SBL and (b) RBL. The *legend* indicates downstream position and the horizontal *dotted line* indicates the rotor axis

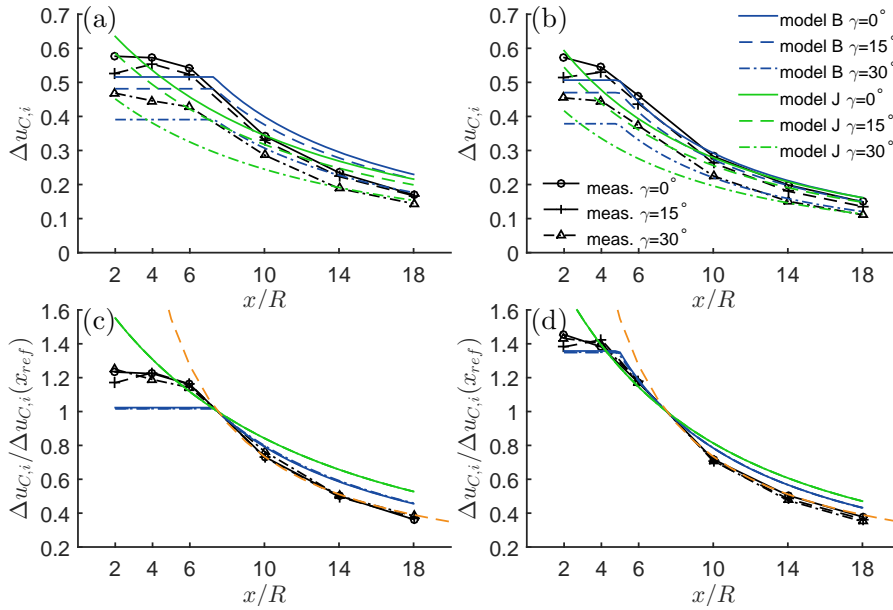
As mentioned before, the yaw angle exhibits little influence on the lateral spreading rate  $k_y = d\sigma_y/dx$ . Therefore, in the following it is assumed that the same holds for the vertical spreading rate. Hence, to compare the models with the measurements,  $k_y$  and  $k_z$  in the linear region of the un-yawed cases are used as input parameter  $\bar{k} = \sqrt{k_y k_z}$  for both models. Figure 7 shows the resulting wake widths predicted by the models  $\bar{\sigma}_B$  and  $\bar{\sigma}_J$  as well as the measured wake width  $\bar{\sigma}_M = \sqrt{\sigma_y \sigma_z}$ . Both models capture the wake width in the linear region well within the two boundary layers. As it can easily be seen, other than Model J, Model B also predicts the change in the wake width due to the yawing, which however is slightly underestimated.

Unsurprisingly the predicted centreline velocity deficit becomes more accurate the closer the predicted wake width is to the measurement results, as it can be seen in figure 8(a) and (b). Despite the fact that in both models the influence of the yaw angle on the wake width is underestimated or even not considered, both models are capable to predict its influence on the centreline velocity deficit correctly. However, the accuracy of the models should not only be evaluated based on how close the prediction is to the results within a certain interval, since this can be easily influenced by tuning the model input parameters. It should also be considered if the models are capable to reproduce the decay rate of the velocity deficit in the far wake. Therefore, in figure 8(c) and (d) the centreline velocity deficit is normalised by the value at



**Figure 7.** Measured (M) and modelled isotropic wake half width  $\bar{\sigma}_i$  with  $i = M, B, J$  in the (a) SBL and (b) RBL. The legend indicates the yaw angle.

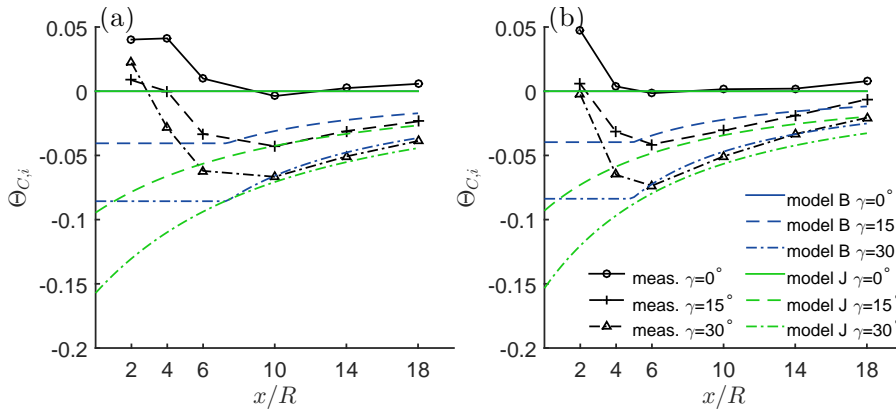
$x_{ref}/R = 7.5$  which for all cases is downstream of the potential core region. The collapse of the measured centreline velocity deficits suggests that these curves follow an universal decay law and are hence independent of the considered yaw angle and flow condition. In both boundary layers the decay of the centreline velocity deficit follows a  $x^{-1}$  law which is shown in the figure as *orange dashed line*. For both models the centreline velocity deficit also becomes independent of the yaw angle and in case of the Model B also independent of the flow condition, respectively ground roughness. Furthermore, Model B comes closer than Model J to the  $x^{-1}$  law of the centreline velocity deficit.



**Figure 8.** Measured (M) and modelled centreline velocity deficit  $\Delta u_{C,i}$  (a), (b) and normalised centreline velocity deficit  $\Delta u_{C,i}/\Delta u_{C,i}(x_{ref})$  (c), (d) in the SBL and RBL respectively, where  $i = M, B, J$ . *Orange dashed line* denotes  $(x/x_{ref})^{-1}$  curve. The legend indicates the yaw angle.

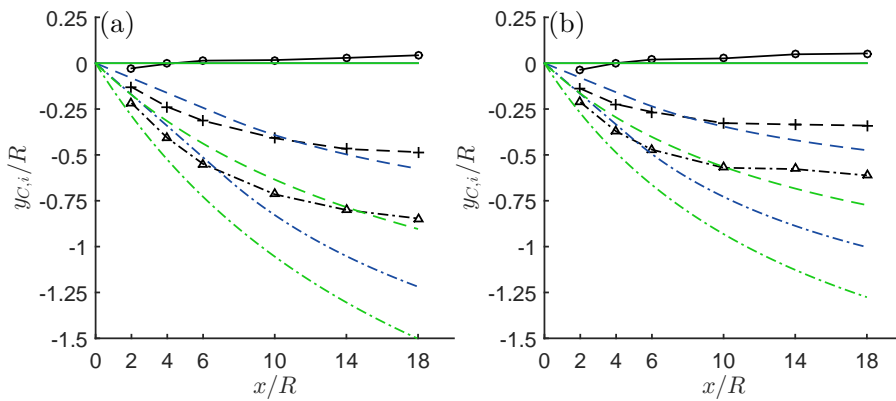
Since both models calculate the wake deflection based on the integration of the modelled centreline skew angle in the downstream direction, figure 9 compares these predictions with the measured values. In general both models give an acceptably accurate prediction on the skew angle in the far wake. Despite the simplicity of the skew angle prediction of Model J eq. (10) compared to Model B eq. (6), the predicted decay rate of the centreline skew angle is quite similar in both models, though they differ in magnitude. However in the near wake Model J predicts an excessive skew angle, whereas Model B limits the skew angle to the constant value  $\Theta_{C,0}$ , which for all cases is close to the measured maximum centreline skew angle.

Figure 10 shows the resulting prediction of the centreline position as well as the measured



**Figure 9.** Measured (M) and modelled centreline skew angle  $\Theta_i$  where  $i = M, B, J$  in the (a) SBL and (b) RBL. The legend indicates the yaw angle.

centreline based on the momentum deficit center in eq. (13). It is evident that Model J overestimates in all cases the lateral wake deflection. Since both models predict similar centreline skew angles in the far wake, the main reason for this mismatch is the excessive skew angle predicted by the Model J in the near wake region as mentioned before. The prediction of Model B however matches the momentum deficit centre quite well for a yaw angle of  $\gamma = 15^\circ$  in both boundary layers. Nevertheless, in the far wake, the relative deflection (deflection between two downstream positions) is overestimated. This becomes especially visible at a yaw angle of  $\gamma = 30^\circ$ , where the assumption of a constant centreline skew angle results in a good prediction of the wake position in the near wake within both boundary layers, the far wake position however is significantly overestimated. Considering the good agreement of measured and modelled centreline skew angle for  $x/R \geq 10$  it seems to be somewhat questionable that the wake centreline can be found by integrating the skew angle eq. (7). As mentioned before this approach implies the centreline to be equal to a streamline.



**Figure 10.** Measured (M) and modelled wake centreline position  $y_{C,i}$  where  $i = M, B, J$  in the (a) SBL and (b) RBL. Legend in Figure 9 gives yaw angle.

To complete the discussion, figure 11 depicts the measured and predicted lateral velocity profiles at several downstream positions for the yaw angles  $\gamma = 0^\circ$  and  $30^\circ$ . Despite the observed deviations in the wake growth, the recovery of the velocity deficit and the wake trajectory, the predictions of Model B are in satisfactory agreement with the measurement results.

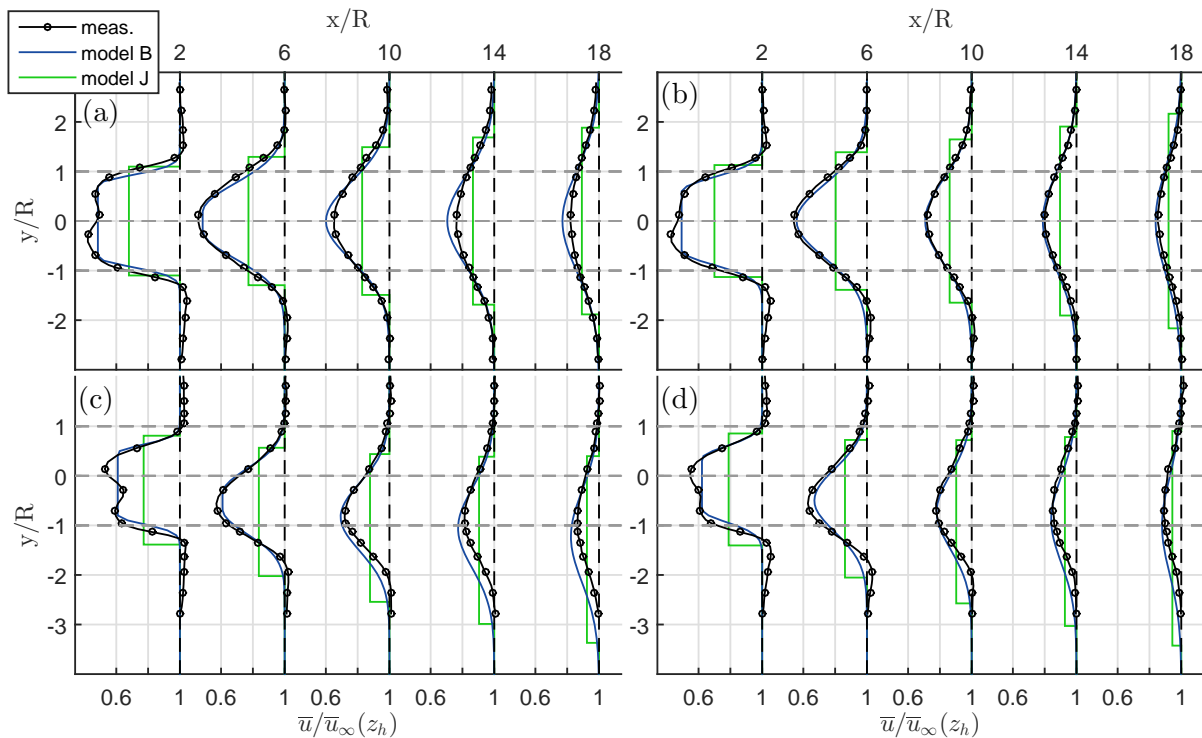


**Figure 11.** Lateral profiles of the measured (*black line*) and modelled (Model B *blue line*, Model J *green line*) velocity in the wake of the model wind turbine immersed in the SBL with (a)  $\gamma = 0^\circ$ , (c)  $\gamma = 30^\circ$  and in the RBL with (b)  $\gamma = 0^\circ$ , (d)  $\gamma = 30^\circ$ .

## 5. Summary

Wind tunnel measurements were performed to investigate the influence of roughness induced turbulence on the wake trajectory of a yawed model wind turbine. It is shown that an increase in the turbulence intensity decreases the lateral wake deflection. Considering yaw misalignment as a control strategy to improve the power production in on-shore windfarms might hence be less beneficial with increasing terrain roughness. It is confirmed that the wake growth rate is the same for different yaw angles whereas it is influenced by the level of the ambient turbulence intensity, respectively ground roughness. Furthermore, it is shown that the measured lateral profiles of the velocity deficit in the far wake become self-similar and exhibit a decay rate close to  $x^{-1}$ , independent of the ambient turbulence intensity and yaw angle. The computational inexpensive analytical wake models derived by Bastankhah & Porté-Agel [3] and Jiménez & Crespo [11] are then tested against the measurement results, using only the wake growth rate as given information from the measured flow fields. It is shown, that both models are capable to reproduce the general trends regarding the wake growth, decay of the centreline velocity deficit and skew angle in the far wake correctly. The assumed Gaussian distribution used to model the velocity deficit in the far wake in [3] matches well the measurement results. Both models however fail to predict the wake trajectory accurately, especially for large yaw angles. Given the accurate prediction of the centreline skew angle, it is hypothesised that the wake centreline can not assumed to be equal to a streamline.

Motivated by the observable degree of self-similarity in the profiles of the mean velocity, future research will focus on the analysis of profiles of Reynolds stresses regarding self-similarity, as well as improving some aspects of the discussed wake models.

## Acknowledgments

This research was supported by the GreenTech Initiative of the Eurotech Universities.

## References

- [1] Fleming P, Gebraad P, Lee S, Wingerden JW, Johnson K, Churchfield M, Michalakes J, Spalart P, Moriarty P 2014 *Renew. Energy* **70**
- [2] Vollmer L, Steinfeld G 2016 *Wind Energ. Sci.* **1** 2
- [3] Bastankhah M, Porté-Agel F 2016 *J. Fluid Mech.* **806**
- [4] Counihan J 1969 *Atmospheric Environment* **3** 197
- [5] Breitsamter C 1997 *Turbulente Strömungsstrukturen an Flugzeugkonfigurationen mit Vorderkantenwirbeln* PhD Thesis, Technical University of Munich, Germany
- [6] Counihan J 1975 *Atmospheric Environment* **9** 871
- [7] Heist D, Castro I 1998 *Experiments in Fluids* **24** 375
- [8] Chamorro L, Arndt R, Sotiropoulos F 2012 *Wind Energy* **15** 733
- [9] Bastankhah M, Porté-Agel F 2017 *Energies* **10** 7
- [10] Stein V, Kaltenbach HJ 2016 *Journal of Physics: Conference Series* **753** 032061
- [11] Jiménez Á, Crespo A, Migoya E 2010 *Wind Energy* **13** 559
- [12] Wu Y, Porté-Agel F 2012 *Energies* **5** 103390
- [13] Jin Y, Chamorro L 2016 *Energies* **9** 10